

# Long-term eddy modulation inhibited the meridional asymmetry of halocline in the Beaufort Gyre

Jinling Lu<sup>1,2</sup>, Ling Du<sup>1,2</sup>, Shuhao Tao<sup>1,2</sup>

<sup>1</sup>Frontier Science Center for Deep Ocean Multispheres and Earth System (FDOMES) and Physical Oceanography Laboratory, Ocean University of China, Qingdao, 266100, China

<sup>2</sup>College of Oceanic and Atmospheric Sciences, Ocean University of China, Qingdao, 266100, China

*Correspondence to:* Ling Du (duling@ouc.edu.cn)

**Abstract.** Under the background of wind forcing change along with Arctic sea ice retreat, the mesoscale processes undergoing distinct variation in the Beaufort Gyre (BG) region are increasingly important to oceanic transport and energy cascade, and then these changes put oceanic stratification into a new state. Here, the varying number and strength of eddies in the central Canada Basin (CB) and Chukchi–Beaufort continental slope are obtained based on mooring observations (2003–2018), altimetry measurements (1993–2019) and reanalysis data (1980–2020). In this paper, the variability in the BG halocline representing the adjustment of stratification in the upper layer is shown to analyse how it occurs under changing mesoscale processes. We find that the halocline depth has deepened by ~40 m in the south of the central gyre while that in the north has deepened by ~70 m in nearly the last two decades according to multiple datasets. Surrounding the central gyre, the asymmetry of halocline, with much steeper isopycnal slope close to southern bathymetry, reduced in the final. In the meantime, eddy activities in the upper layer from the southern margin of BG to the abyssal plain have been enhanced. Moreover, eddy-induced convergence of low-salinity water transportations has increased as halocline structures on either side of the central gyre reached a nearly identical and stable regime. It was clarified that the long-term dynamic eddy modulation through eddy fluxes facilitating the freshwater redistribution inhibited the meridional asymmetry of the BG halocline. Further research into reconciling high-resolution observations and data simulations can provide a better understanding of the eddy modulation processes and their influence on large-scale circulation.

## 1 Introduction

Global temperatures have continued to rise since the 1970s. The Arctic Ocean, as the focal point of climate change research, is the region with the most dramatic global surface temperature warming (Huang et al., 2018), with a warming range as high as 1.2 °C/10a, more than twice the global average warming range, which is called the “Arctic amplification” phenomenon (Serreze and Barry, 2011). These variations not only affect the upper ocean circulation but also expose the Arctic atmosphere–ice–sea system to rapid changes (Moore et al., 2018; Timmermans and Marshall, 2020). In this context, with summer sea ice declining in the Arctic (Stroeve et al., 2007, 2014; Niederrenk and Notz, 2018), the presence of increased freshwater in the upper layer alters local stratification, resulting in the variability of water masses. Meanwhile, increased active ocean–

atmosphere interactions and mesoscale processes in the Canada Basin (CB) due to the emergence of broader open areas have attracted increasing attention.

The Beaufort Gyre (BG) in the CB, a large-scale wind-driven anticyclonic circulation feature, that stores a substantial amount of freshwater in the CB (Proshutinsky et al., 2009, 2019), is accompanied by prevalent mesoscale eddies (Doddridge et al., 2019; Manucharyan and Spall, 2016; Zhao and Timmermans 2015; Zhao et al. 2016). The freshwater content (FWC) accumulated by Ekman convergence increased between 2003 and 2008 and remained relatively constant between 2008 and 2012 (Timmermans and Toole, 2023). The halocline in the CB, a thick layer with a double peak of stratification, is considered an insulating “density barrier” between the surface mixed layer and the Atlantic water layer underneath (Bourgain and Gascard, 2011). Observations indicated that the Pacific Winter Water (PWW) layer, a main component of the western Arctic halocline (Shimada et al., 2005), generally deepened during 2004–2018 while isopycnal layer thickness increased (Kenigson et al., 2021). Likewise, there was an isopycnal deepening by 70 m during 2004–2011 (Zhong et al., 2018), suggesting a spin-up of the gyre. The shape of BG is highly asymmetrical and associated with surface forcing (Regan et al., 2019). Furthermore, the asymmetrical stratification and halocline vertical structure in the BG have received attention in recent studies (Kenigson et al., 2021; Zhang et al., 2023). Isopycnals are steeper near the gyre edge than the interior due to topography, indicating stronger baroclinic instability (Manucharyan et al., 2016; Manucharyan and Isachsen, 2019). Isohalines are steeper in the south and east than in the north and west (Zhang et al., 2023). This asymmetrical structure is related to topography, BG strength, and some other factors remaining to be solved.

Previous works on eddies in the CB or the Arctic Ocean were mostly based on satellite products (e.g., Kozlov et al., 2019; Kubryakov et al., 2021, Raj et al., 2016), in situ hydrographic data (e.g., Fer et al., 2018; Timmermans et al., 2008; Zhao et al., 2014, 2016; Zhao and Timmermans, 2015), and high-resolution, eddy-resolving simulations (e.g., Reagan et al., 2020; Wang et al., 2020). Eddy activity, a common feature in the BG halocline, has also been the focus of many past studies. Eddies are mainly concentrated in the subsurface (30–300 m) even though they can extend to thousands of metres in depth (Zhao et al., 2014; Zhao and Timmermans, 2015), due to eddy dissipation by ice–ocean drag in the surface boundary layer (Manucharyan and Stewart, 2022). Moreover, the kinetic energy of mesoscale eddy activities is dominant in the BG halocline (Zhao et al., 2016, 2018). For example, based on 127 eddies observed at drifting sea ice stations, Manley and Hunkins (1985) found that the eddy kinetic energy (EKE) accounted for approximately one-third of the total kinetic energy of the upper 200 m in the CB. The depth of EKE maximum value is generally found at approximately 70–110 m in the halocline (Wang et al., 2020). From the perspective of horizontal patterns, the southern CB is popular with a large number of cold-core and anticyclonic halocline eddies (Spall et al., 2008). Zhao et al. (2016) kept Ice Tethered Profiler (ITP) measurements between 2005 and 2015 to survey the changes in the eddy field in the CB. They found that eddies were mostly distributed in the western and southern parts of the CB. EKE derived by satellites is also higher along the major boundary currents and continental shelves in the Arctic Ocean (Timmermans and Marshall, 2020; Wang et al., 2020).

In this paper, we focus on the long-term variability of eddy activity to associate it with oceanic stratification. According to previous works, the number of eddies in the lower halocline doubled from 2005–2012 to 2013–2014 (Zhao et al., 2016), with

65 the past increase before 2007 in FWC and gyre strength (Regan et al., 2019; Timmermans and Toole, 2023), and a stabilisation since 2008 (Zhang et al., 2016). The response of EKE to the spin-up of the gyre during 2003–2007 showed that EKE at the subsurface has generally strengthened (Regan et al., 2020). Recent research has also demonstrated that with wind energy input increasing into the BG due to the significant loss of sea ice after 2007, eddy activities would also be more active (Armitage et al., 2020).

70 In addition to the spatiotemporal variations of the eddy field, the influence of eddy activity has also received extensive attention. Global mesoscale eddies can transmit momentum, heat and water masses, contributing to atmospheric circulation and mass distribution as well as acting in ocean heat balance (Chelton et al., 2007). Eddies not only exhibit unprecedented changes but also play a crucial role in the Ekman-driven BG stability in the context of sea ice loss (Manucharyan et al., 2016). They can balance atmosphere–ocean and ice–sea stress input, gradually weaken the isopycnal slope and geostrophic currents and

75 counteract the accumulation of FWC driven by Ekman pumping by dissipating available potential energy (APE) (Manucharyan and Spall, 2016). In addition, Ekman pumping and sea ice are also major factors affecting BG halocline dynamics. This balance between halocline and eddies is thought to occur on different time scales in realistic models, which suggests a link between small-scale features and changes to large-scale circulation (Doddridge et al., 2019; Manucharyan et al., 2017). However, with sea ice conditions changing due to global warming, the long-term variability of eddies in the central basin and

80 basin boundary regions is still unsolved. Furthermore, according to the standpoints about possible gyre stabilisation and asymmetrical halocline in recent years (e.g., Proshutinsky et al., 2019; Zhang et al., 2016, 2023), the eddy modulation in the asymmetrical halocline structure on a long timescale is still unknown. Due to influence of the measurement conditions and limited satellite observations, continuous eddy observation data in space and time are relatively scarce. Data coverage in space and time has yet to be improved (Zhao et al., 2016). The results of numerical simulations lack effective data to support them,

85 so research on oceanic mesoscale eddies remains uncertain to some extent. Here, we use multiple datasets containing moored, in situ, and satellite altimetry observations, in comparison with reanalysis data, to quantify the strength of eddies by sea level anomaly (SLA) and horizontal currents. The stationary eddies and EKE, as well as the variability of the halocline structure, are both noted to assess the deformation of the asymmetrical halocline in the BG under the changing eddy modulation. Section 2 presents the details of the data and methodology. Section 3 demonstrates the variability of the entire halocline layer,

90 especially on its meridional asymmetry in the BG region. The eddy distribution and long-term changes are discussed in section 4. Section 5 explains significant eddy modulation in the halocline structure as well as the correlation between EKE and geostrophic currents. Section 6 is the summary and discussion of this paper.

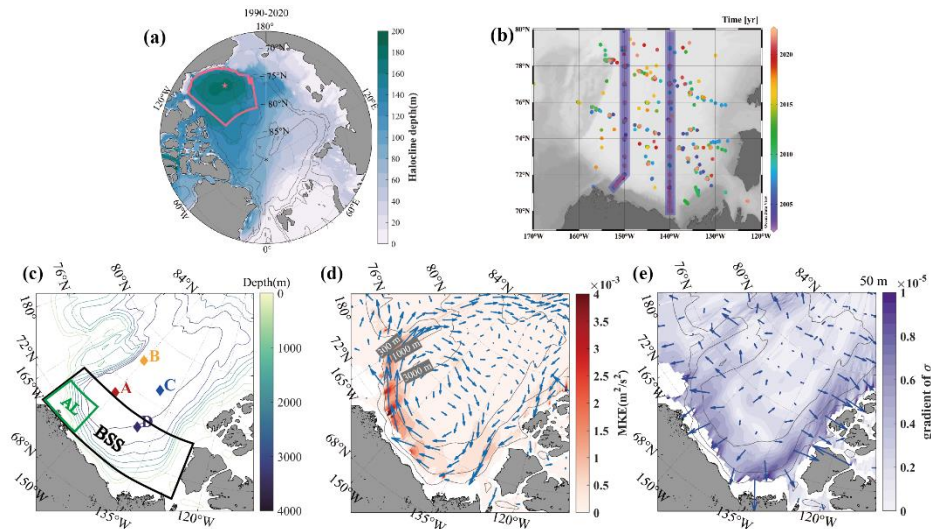
## **2 Data and methods**

### **2.1 Observations and ocean reanalysis data**

95 In this paper, we use multiple datasets, including hydrographic observations, satellite altimetry, and reanalysis datasets. The hydrographic data are in situ measurements from CTD and mooring observation from McLane Moored Profilers (MMPs) at

four moorings that are all deployed under the Beaufort Gyre Exploration Project (BGEP). The reanalysis datasets used here mainly consist of World Ocean Atlas 2023 (WOA23) and Simple Ocean Data Assimilation (SODA, version 3.4.2).

An annual hydrographic survey through ship-based CTD has been conducted in the BG region each year between August and October. CTD data between 2004 and 2021 are mainly used to investigate the spatiotemporal variability in oceanic stratification across the fundamental BG region (Fig. 1a). The positions of the deployed CTD instruments are shown in Fig. 1b. Additionally, to supplement the long-term trends and changing characteristics of the halocline and to capture mesoscale eddies at representative stations in the CB, mooring data deployed at four corners around the basin (Fig. 1c) between mid-2003 and mid-2018 above 500 m are also analysed. Each mooring system included a MMP that returns profiles of horizontal velocity, temperature, salinity, pressure, etc. A pair of upgoing/downgoing profiles (separated by 6 hours) is returned every other day, and the data are processed to a vertical resolution of 2 dbar. The shallowest moored measurement varies from approximately 50–90 m (depending on the mooring and sampling period) to avoid collisions with ice keels, and the deepest measurements are 2000 m.



110 **Figure 1.** (a) A map of climatology halocline depth. Pink box and star indicate the BG area and center, referring to Regan et al. (2020). This BG box is defined as the region between 70.5–80.5°N and 170–130°W, bounded by the 300 m bathymetry. The center of the mean gyre from 1990 to 2014 is situated at 74.74°N and 150.62°W. (b) The positions of in situ sites of CTD measurement from BGEP in certain months during 2004–2021. The purple bars indicate two meridional transects with a width of 36 km mostly along 150°W and 140°W. (c) A map of the Canada Basin and the bathymetric contours above the 4000 m isobath. Coloured diamonds denote the locations of four BGEP moorings. The two chosen regions are shown by green (AL, Alaskan coast) and black (BSS, Beaufort Sea slope) boxes. (d) The distribution of mean kinetic energy (MKE) at 50 m. Vectors denote the direction of mean currents. Grey lines denote the 300 m, 1000 m, and 3000 m bathymetry. (e) The distribution of horizontal gradient of potential density (shading) at 50 m. Vectors point in the direction of increasing potential density. The results of (a), (d), and (e) are calculated from the 1990–2020 WOA climatology.

120 The SODA reanalysis is developed by the University of Maryland based on the Global Simple Ocean Data Assimilation System, which is the 5-day average from 1980 to 2020 adopted in this paper, with a horizontal resolution of  $1/2^\circ \times 1/2^\circ$  and vertically

divided into 50 layers with unequal spacing. We obtain gridded altimetry data (product identifier: SEALEVEL\_GLO\_PHY\_L4\_REP\_OBSERVATIONS\_088\_047) over the years 1993–2019 from the Copernicus Marine Environmental Monitoring Service (CMEMS). This product consists of daily gridded maps of dynamic topography in ice-free regions that have been derived as a sum of mapped SLAs calculated from combined measurements by different satellites and mean dynamic topography (MDT) (Kubryakov et al., 2021).

## 2.2 Methods

To estimate EKE and assess the strength of eddy activities, we use ocean current data from SODA and altimetry. Geostrophic velocities are calculated from sea level height. The horizontal velocity is deconstructed into annual mean velocity ( $\bar{u}, \bar{v}$ ) and anomaly ( $u', v'$ ) (Penduff et al., 2004; Rieck et al., 2015, 2018; Regan et al., 2020):

$$u = \bar{u} + u', v = \bar{v} + v',$$

$$\text{and then } EKE = (u'^2 + v'^2)/2. \quad (1)$$

Note that the EKE in this paper is estimated by a low-frequency ‘‘eddy’’, which is defined as a departure from a long-term temporal mean, with a period (depending on the temporal resolution of the data) of greater than 5 days or 1 day (Lucke et al., 2017). In addition, the vertical velocity shear  $\partial \mathbf{U} / \partial z$  can be related to the large-scale density field by the thermal wind relation

$$\frac{\partial \mathbf{U}}{\partial z} = \frac{g}{f_0 \rho_0} \frac{\partial \rho}{\partial z} \vec{k} \times \nabla_{z\rho} = \frac{N^2}{f_0} \vec{k} \times \nabla_{z\rho} \quad (2)$$

where  $\mathbf{U}$  is the horizontal current field,  $N$  is the Brunt-Väisälä buoyancy frequency, which represents oceanic stratification,  $\nabla_{z\rho} = (-\frac{\partial \rho}{\partial x} / \frac{\partial \rho}{\partial z}, -\frac{\partial \rho}{\partial y} / \frac{\partial \rho}{\partial z})$  is the isopycnal slope,  $\rho$  is the potential density of seawater,  $\rho_0$  is the average density of seawater,  $g$  is the gravity acceleration, and  $z$  is depth (Meneghello et al., 2021). Developed by Eq. (2), the horizontal velocity field is calculated by integration with depth from bottom to surface. As maps of the horizontal velocity field (Fig. 1d) and density gradient (Fig. 1e) at 50 m in the CB show, the main circulation feature is discerned, and the southwestern basin near continental slopes is the key region for varying currents tending towards high EKE and instability.

To investigate the variation in the overall halocline and understand the shifting of oceanic stratification, we consider the depth of the potential density surface  $\sigma=27.4$  (25)  $\text{kg}\cdot\text{m}^{-3}$  to approximately represent the base (top) of the entire halocline layer (Timmermans et al., 2020). Accordingly, the depth of the surface mixed layer is also identified by the halocline upper boundary (Bourgain and Gascard, 2011; Polyakov et al., 2018). Based on the upper and lower boundary of the halocline, APE is defined as the amount of potential energy in a stratified fluid available for mixing and conversion into kinetic energy (Huang 1998; Munk and Wunsch 1998). The calculation of APE here is following Eq. (3):

$$APE = PE - PE_{ref} = \iiint_{z_{ref}}^{surface} g[\rho(z) - 1027.4]z dz dA, \quad (3)$$

where  $z_{ref}$  represent the depth of the halocline lower boundary, and  $A$  is the gyre area (Armitage et al., 2020; Bertosio et al., 2022; Polyakov et al., 2018).

Furthermore, to discern the critical role of mesoscale eddies in balancing the halocline, we consider that the eddy advection velocity in the (y, z) plane can be defined from an eddy stream function  $\psi^*$  as

$$v^* = -\psi_z^*, w^* = \psi_y^* \quad (4)$$

155 and  $\psi^*$  is represented as

$$\psi^* = \frac{\overline{v'S'}}{\overline{S_z}} = -\frac{\overline{w'S'}}{\overline{S_y}} \quad (5)$$

where  $\overline{v'S'}$  is the average meridional eddy salt flux and  $\overline{S_z}$  is the average vertical salt gradient (Manucharyan et al., 2016; Manucharyan and Spall, 2016; Manucharyan and Isachsen, 2019; Marshall and Radko, 2003). Here, bars and primes correspond to the annual mean and perturbation variables. Because buoyancy is mainly controlled by salinity in the Arctic,  $\psi^*$  represents the cumulative effects of eddy thickness fluxes that arise from correlations between eddy velocities and eddy-induced isopycnal displacements. Overall, when the vertical salt gradient is generally negative in the CB, a positive value of  $\psi^*$  indicates southwards (northwards) transportations of low-salinity (high-salinity) water and vice versa.

If eddy genesis is related to baroclinic instability, the baroclinic growth rate  $\omega$  is correlated with EKE. The baroclinic growth rate  $\omega$  can be estimated here by

$$165 \quad \omega = f \sqrt{\frac{1}{6H} \int_H^0 \frac{dz}{R_i(z)}} \quad (6)$$

where  $R_i = N^2 / [(\frac{\partial u}{\partial z})^2 + (\frac{\partial v}{\partial z})^2]$  is the Richardson number (Smith, 2007). We call the inverse of this quantity  $\omega^{-1}$  the ‘‘Eady timescale’’. The Eady timescale should be short where there is anomalously high EKE or weak stratification.

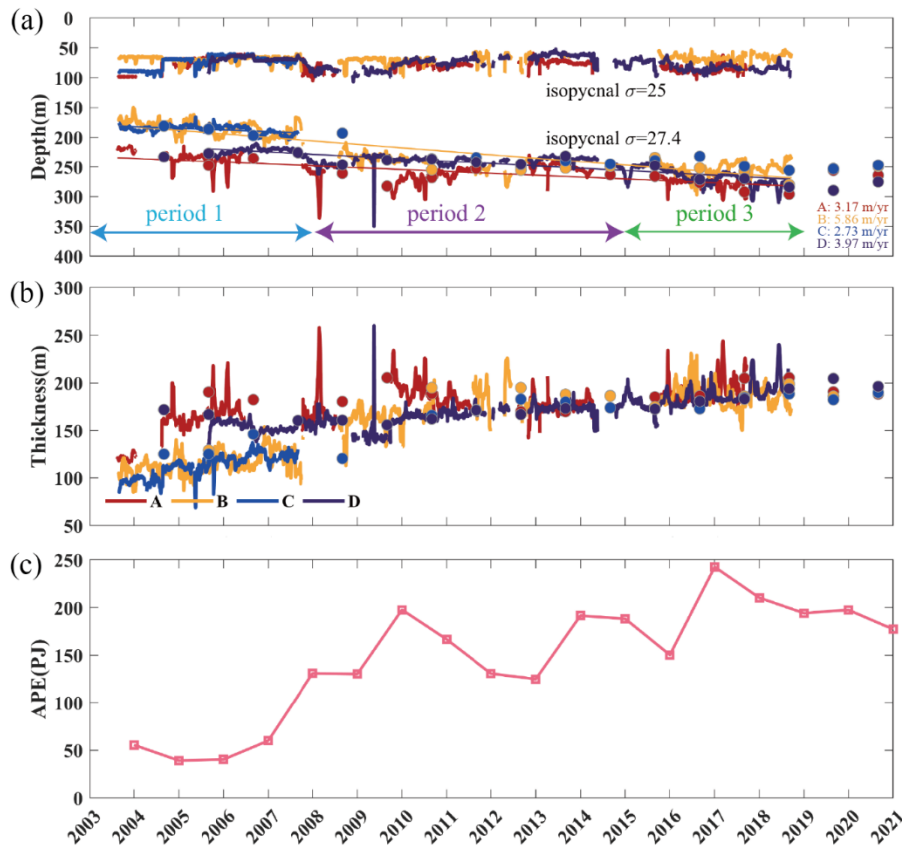
### 3 BG halocline variability

In this section, we aim to investigate the spatiotemporal variability in the halocline in the BG region, particularly its varying asymmetry inside, which is the focus of this article. The halocline’s depth, thickness and strength, and vertical structure are analysed in detail below, all of which indicate its meridional asymmetry.

#### 3.1 Temporal variation in the halocline

With the spin-up of the BG, the isopycnals of the PWW layer in the cold halocline have deepened (Kenigson et al., 2021). We chose the 25 and 27.4 isopycnal surfaces to characterize the halocline top and base. Figure 2 shows the discontinuous variation in the halocline upper/lower boundary and thickness at four moorings from MMP. The depth of the surface mixed layer is less than 70 m. The entire halocline layer underneath the mixed layer, including upper and lower halocline, is mainly at 70–250 m. To supply the lack of MMP measurements, the annual means of halocline depth and thickness are also analysed based on CTD. Compared with MMP results, the mean relative errors of CTD on halocline depth (thickness) are 2.0% (3.4%), 4.4% (7.0%), and 1.0% (3.0%) for moorings A, B, and D, respectively. Given that the rangeability of the halocline top is much smaller than that of the halocline base, and the depth of the halocline upper/lower boundary at a single mooring shows consistent trends,

we mainly focus on the variation in halocline base. There are different characteristics of variation during 2003–2018 despite a lack of measurements over time. The finite MMP results at mooring C showed a deepening trend in the halocline depth and increased thickness before 2008, well overlapped with mooring B. In addition, other moorings provided results over a longer term, which captured a deepening of the halocline base and an increase in thickness over the years from 2003 to 2018. The thickness of the halocline at mooring B in the northwestern part of CB increased steadily by approximately 70 m; moreover, the depth of the halocline base deepened by up to 70 m over the years 2003–2018. The thickness of the halocline in the southern part of the basin (moorings A and D) increased by approximately 30 m with the halocline base deepening by approximately 40 m. Notably, the depth of the halocline had a stagnant phase and even shallowing development over the years 2008–2014. Linear trends and mean values of the halocline depth and thickness in three periods (2003–2007; 2008–2014; 2015–2018) are computed (Table 1). A shallowing trend of halocline depth is clear during 2008–2014 in the southern sites of the basin (moorings A and D), but the former and latter periods both mostly exhibit deepening trends in halocline depth. The variations at northern sites (moorings B and C) covering three periods are similar, which show entirely different features from southern sites. The halocline depth continues deepening over the whole period. The halocline thickness and depth between every site tend to be at a nearly identical level in the final period and those differences are smaller than in the first period.



195

200 **Figure 2. Time series of (a) depth of isopycnals 25 kg/m<sup>3</sup> (upper coloured lines) and 27.4 kg/m<sup>3</sup> (lower coloured lines) representing the top and base of the halocline, and (b) halocline thickness between isopycnals 25 kg/m<sup>3</sup> and 27.4 kg/m<sup>3</sup> for moorings A, B, C, and D during 2003–2018. Long-term deepening trends of depth of halocline base are tagged. Note that the anomalies record eddies were existent at that time. Coloured dots indicate the annual means near the four moorings derived from CTD. (c) Annual means of APE in the BG box calculated from CTD.**

APE, a good integral indicator of changes in overall halocline strength in the BG box, is also computed here by Eq. (3) using CTD surveys. As shown in Fig. 2c, there was a significant increase from ~50 to ~200 PJ before 2010. However, APE was continuously decreasing in the periods of 2010–2013, 2014–2016 and 2017–2021, meaning a flattening of isopycnals in the BG and APE release. Although there was a short-term increase in APE accumulation in 2016–2017, it did not lead to further accumulation, indicating an energy reservoir limit around 150–250 PJ. We infer the variabilities in the halocline and APE have a relationship with the BG spin-up and the largest increase in FWC during 2003–2007 (Giles et al., 2012; Krishfield et al., 2014; Timmermans and Toole, 2023). Additionally, halocline depth and thickness remained stagnant in the post spin-up term during 2008–2014 (Regan et al., 2020).

210 **Table 1. Trends (within the brackets, unit: m/yr) that all pass significant tests (confidence level 99%) and mean depth (outside the brackets, unit: m) of the halocline top, base, and halocline thickness in three periods for moorings A, B, C, and D.**

Moorings		Periods		
		2003–2007	2008–2014	2015–2018
A	top	75.4(-2.7)	77.8(-2.0)	86.2(-1.2)
	base	236.4(7.3)	261.1(-4.5)	278.1(7.9)
	thickness	161.0(10.0)	183.3(-2.5)	191.9(9.1)
B	top	69.1(0.5)	69.8(-2.0)	66.8(-1.1)
	base	184.1(4.9)	241.1(5.4)	252.6(3.6)
	thickness	115.0(4.5)	171.3(7.3)	185.8(-2.4)
C	top	74.3(-5.7)		
	base	186.5(2.7)		
	thickness	112.3(8.5)		
D	top	69.3(2.2)	73.6(-3.9)	81.5(3.1)
	base	223.7(0.4)	239.4(-0.4)	267.6(8.9)
	thickness	154.4(-1.8)	165.9(3.6)	186.1(5.8)

### 3.2 Changes in the meridional asymmetry of the halocline

The stratification in BG region is marked by pronounced asymmetry, as highlighted by Zhang et al., (2023). The isopycnal slope is steeper over the southern continental slope than in the northern basin (Fig. 1e), which is in line with previous research



215 (e.g., Proshutinsky et al., 2019; Regan et al., 2019; Zhang et al., 2023). In section 3.1, we observe that there are significant differences in the evolution of the halocline between the north and south of the basin, which deviates slightly from previous findings. Earlier research has shown that isopycnals deepened at different rates in the northwestern and southeastern parts of the basin during 2002–2016 (Zhong et al., 2019). However, our analysis reveals a more noticeable meridional difference between the north and south. To gain a comprehensive understanding of the asymmetric halocline across the fundamental BG

220 box, we utilize inhomogeneous gridded in situ hydrographic data from the latest CTD survey (Fig. 1.a). By examining the horizontal maps in three distinct periods (Fig. 3), determined based on the trends of halocline depth and thickness at the moorings, we see evident changes in the horizontal patterns of the halocline depth. This suggests a transformation of oceanic stratification in the upper layer. In the initial period, the halocline base maps highlight significant differences between the north and south. And then the north experiences a much more pronounced deepening of the halocline depth compared to the south

225 closer to the Beaufort Sea slope, which also exhibits more fresher water. In the final period, the area with the maximum halocline depth is located in the abyssal plain between the Canadian Arctic Archipelago and Northwind Ridge.

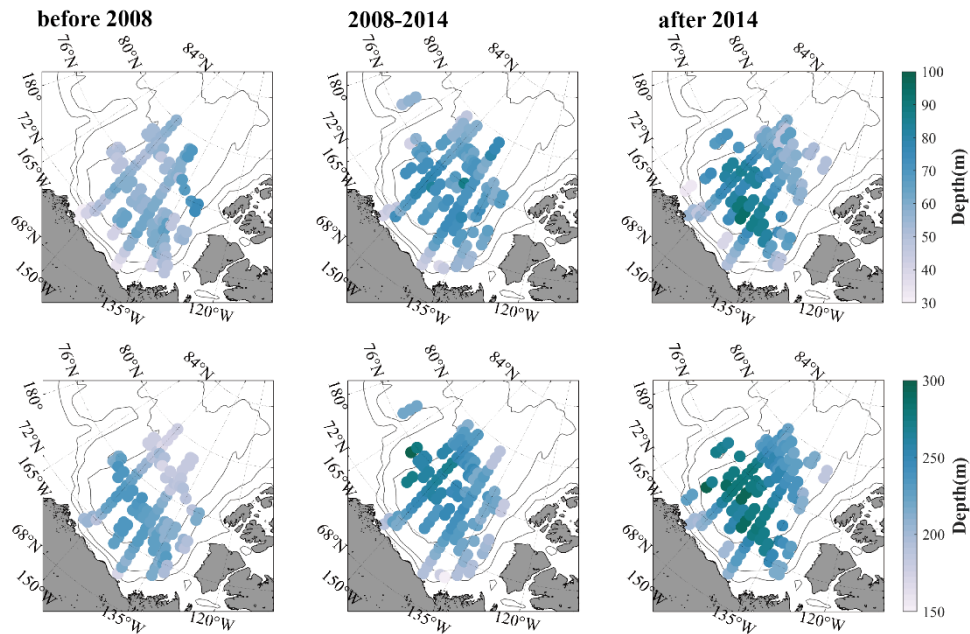
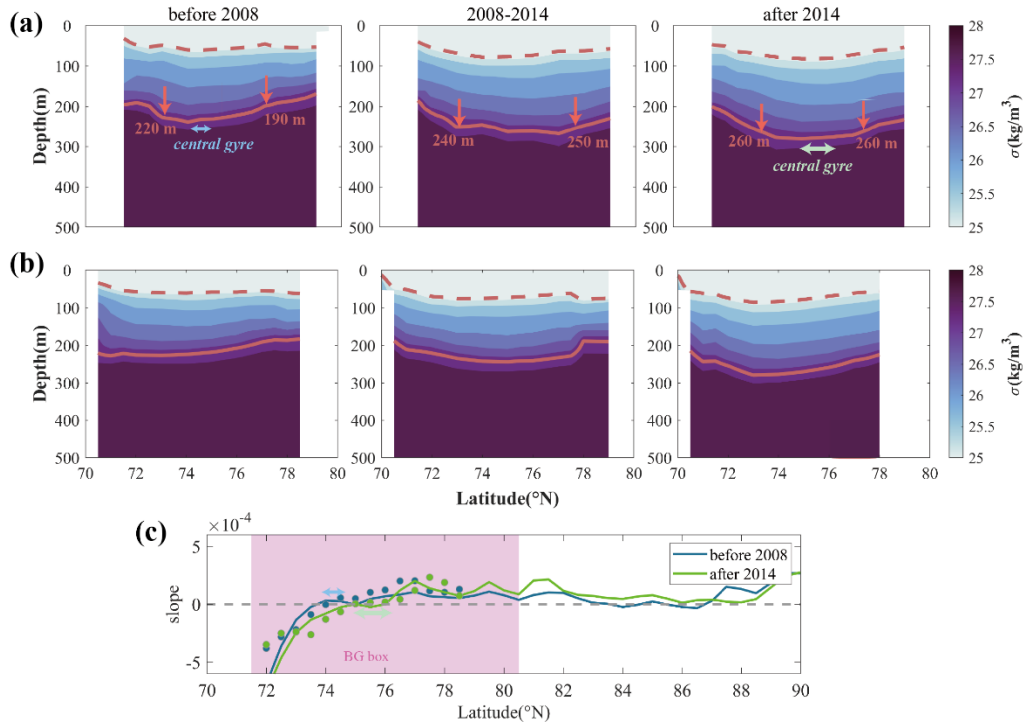


**Figure 3. Horizontal distribution of the depth of halocline (upper panel) top and (lower panel) base across the Beaufort gyre region averaged in 2004–2007 (before 2008), 2008–2014, and 2015–2021 (after 2014).**

230 According to the movements of the gyre center mainly between 140°W and 150°W over 2003–2014 (Regan et al. 2019), we select two north–south transects along 140°W and 150°W (Fig. 1b), which both traverse the deepest part of the BG halocline (Fig. 1a), and make a comparison. The in situ hydrographic data are interpolated onto the regular grids to examine the varying vertical structures of the isopycnals along the selected transects. We find that the hydrographic structures from the two transects have similar features (Fig. 4), which is the same as the former study (Timmermans and Toole, 2023). From the views of the

235 two transects, the halocline thickness was relatively thicker in the south than in the north before 2008. However, the change is more significant and the halocline layer is much thicker along 150°W than along 140°W. Thus, we emphasise the shifts in halocline structures along the 150°W transect. The vertical distribution of the isopycnal  $\sigma = 27.4 \text{ kg} \cdot \text{m}^{-3}$  surface show that it is shallowest  $\sim 200 \text{ m}$  at the margins of the BG region and up to  $80 \text{ m}$  deeper in the interior in the final period (Fig. 4). Based on SODA reanalysis, the isopycnal fluctuation in the halocline is remarkable just in the south of approximately  $82^\circ\text{N}$  but negligible in the far from BG region (Fig. S1). The much steeper isopycnal slope near about  $90^\circ\text{N}$  is due to an overall weakening stratification in the Eurasian Basin that is different from in the CB. In the BG box, where halocline is deepest and its slope is obvious, variability on main part of BG halocline is well captured in spite of northern limit of observation.



245 **Figure 4. Vertical transects along (a) 150°W and (b) 140°W of interannual mean potential density using data from CTD measurements in 2004–2007 (before 2008), 2008–2014, and 2015–2021 (after 2014). The dashed (solid) lines indicate the depth of  $\sigma = 25$  ( $27.4$ )  $\text{kg} \cdot \text{m}^{-3}$  representing the the halocline top (base). The depths of halocline base on either side of central gyre are marked in the upper panel. (c) Meridional slope of isopycnal  $\sigma = 27.4 \text{ kg} \cdot \text{m}^{-3}$  in first and last periods from SODA (solid line) and CTD (dot).**

250 Among the three periods, the vertical structures of isopycnals, especially the lower boundary of the halocline layer, reveal apparent changes between the marginal and interior gyre. Initially, the location of central gyre determined by isopycnal slope of near zero in the interior, was very close to the vicinity of continental slopes with the largest isopycnal steepening occurring to the southern side and stronger baroclinic instability (Manucharya and Isachsen, 2019). There was a gradual uplift of the halocline beyond the northern edge of BG. The obvious meridional symmetry in the halocline can be explained by the intrusion of Atlantic water and strong Ekman downwelling in the central BG (Karcher et al., 2007; McLaughlin et al., 2004; Timmermans and Toole, 2023). The depth of halocline base was deeper by approximately  $30 \text{ m}$  and halocline layer was thicker

255 in the southern side ( $\sim 73^\circ\text{N}$ ) of central gyre than in the north ( $\sim 77^\circ\text{N}$ ). The difference between the north and south was  
narrowed with isopycnals generally deepening from the view of the average vertical structure during 2008–2014, and even the  
northern halocline was deeper than the southern district. In the final period (after 2014), the halocline depth changed less in  
comparison with the previous periods. The location of BG center moved to the north, which was supported by observations  
and SODA reanalysis (Fig. 4c). In the mean time, the halocline steepness reduced close to gyre center and the entire halocline  
260 layer inflated (Zhang et al., 2023), corresponding with stable development in the APE of BG system after a significant  
accumulation (Fig. 2c). Additionally, the halocline depth and thickness tended to be meridionally symmetrical accompanied  
by flattened isopycnal slope surrounding central gyre, shaped like a horizontal bowl under the forcing of surface Ekman  
convergence (Manucharyan and Spall, 2016), indicating that it had reached a state of stabilisation (Zhang et al. 2016). As seen  
from the spatial maps and vertical structures of the halocline, meridional asymmetry reduced in the final period. We infer there  
265 are other physical processes contributing to the variability.

#### 4 Spatiotemporal variability in eddy activity

As revealed in previous research, a regime shift of the BG occurred in 2007–08, with a spin-up phase of the gyre from 2003  
to 2007 and stabilisation after 2007 (e.g., Regan et al., 2020; Zhang et al., 2016). With BG spin-up and regional sea ice retreat,  
mesoscale eddies are responding to dissipate extra energy input and influence the energy redistribution (Armitage et al., 2020).  
270 It is speculated that the eddy genesis is related to APE accumulation and release in the BG region, which can influence the  
vertical structure of the internal halocline (Manucharyan and Spall, 2016; Manucharyan et al., 2016). In the final period, the  
developments of meridional asymmetry in the halocline layer and APE within the BG box have been inhibited. Under this  
background, the spatiotemporal variability in eddy activity, needed for a comprehensive understanding, is discussed in this  
section.

##### 275 4.1 Eddy detection and variation

We outline how mesoscale eddies can be detected based on moored observations. When eddies occur locally, there are strong  
horizontal velocities accompanied by isopycnal displacements. For anticyclonic (cyclonic) eddies, the isopycnals are convex  
(concave). We distinguish horizontal speeds larger than 10 cm/s after removing background currents and isopycnal  
displacements, which are both criterion used in the past literature (Timmermans et al., 2008; Zhao et al., 2014; Zhao and  
280 Timmermans, 2015). In all, 37, 40, 7 and 43 eddies are detected above 500 m at moorings A–D. Similar to previous works  
(e.g., Zhao et al., 2014; Zhao and Timmermans, 2015), in most instances, the temperature/salinity anomalies and convex  
isopycnal displacements in the eddy core are pervasive. Cold-core eddies account for 61.4%. A total of 98% of eddies are  
anticyclones and only three eddies detected at mooring C are cyclones. The cold-core anticyclones are common in the BG  
region due to large-scale dominant anticyclonic circulation coupled with oceanic stratification, where cold and fresh Pacific  
285 water overlies warm and salty Atlantic water. Furthermore, for mooring C, which is less controlled by the BG, with weaker

mean flows (Fig. 1), the characteristics of eddies there are different from others. Some of the eddies are cyclones that are seldom discovered at other moorings. Cyclone existence is related to frontal instability near 80°N, which contributes to cyclone formation (Manucharyan and Timmermans, 2013; Timmermans et al., 2008).

In addition, we confirm annual mean days of existing eddies and counts of warm-core and cold-core eddies over 500 m through moored observations. The interannual variations in days of recording mesoscale eddies and the counts of eddies are highly similar at moorings A and B, and several respective peaks are predominant (Fig. 5, days of effective observations exceed 200 days in most eddy-rich years). The days of eddy activities demonstrate considerable interannual fluctuations. Over the whole period, 2005, 2009, 2013 and 2017 for mooring A are eddy-rich years; for mooring B, 2005, 2009 and 2018 (144 days record valid observations) are eddy-rich years, which is affected by spatial inhomogeneity of eddy distribution or eddy transportation from the southern BG region (Armitage et al., 2020), the key area for eddy generation (Kubryakov et al., 2021; Manucharyan and Isachsen, 2019; Zhao et al., 2014). After 2014, eddy activities at mooring A (B) were more active than the medium period 2009–2014 (2010–2014) when there was a decreasing trend in eddy days. Despite the eddy days for mooring D showing a smaller fluctuation than other moorings, the amplitude of eddy number is noticeable. The in situ measurements at mooring D also capture a considerable amount of mesoscale eddies, with a decreasing trend in eddy number during the medium term 2009–2014 in line with other moorings.

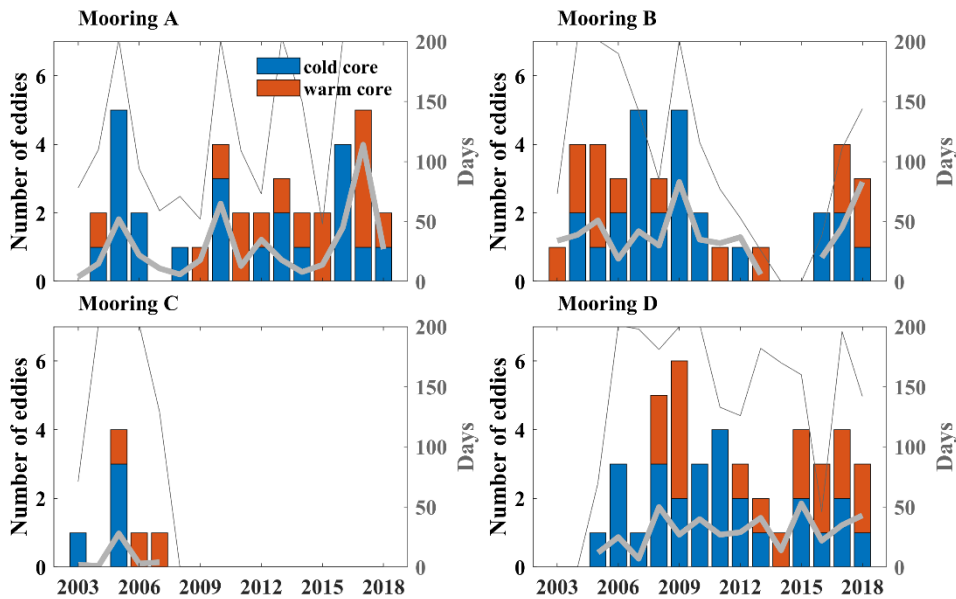


**Figure 5. Interannual evolution of the days of existing eddies (thick grey line) and number of eddies (bar) for four moorings. The blue and red bars indicate the counts of cold-core and warm-core eddies, respectively. Thin grey lines signify the days of recording valid observations in every year.**

Eddies are common between the upper and lower halocline boundaries (Fig. 6a). Additionally, comparing the vertical structures of EKE along with kinetic energy of individual eddies ( $KE_{\text{eddy}}$ ) profiles in three periods at the moorings,  $KE_{\text{eddy}}$

accounts for  $\sim 50\%$  of EKE (Fig. 6b). EKE, as a measurement for eddy strength, can well replicate the main feature of  $KE_{\text{eddy}}$  profiles. EKE changes significantly above the halocline in the three periods, while below the halocline layer, it is relatively weaker, and its multiyear variation is much smaller. The vertical structures of EKE in the basin and its marginal seas can be classified into two types. The first type is that EKE is up to  $\sim 0.01 \text{ m}^2/\text{s}^2$  under the surface mixed layer and decays with depth. The second type is with maximum value at the subsurface of approximately 70–250 m between the upper and lower halocline boundaries. In the first period, EKE above the BG halocline remained at a relatively low level. The results from three moorings (all except mooring C are detected after 2008) showed that EKE was strengthened to varying degrees, accompanied by a deepening of the halocline lower boundary. At the southwestern corner (mooring A) of the basin, only three eddies were detected in the first period. EKE increased in the second period when there were 15 eddies and remained stable in the third period with 13 eddies. Northwestern (mooring B) EKE was stronger with 14 eddies in the second period than before, despite 17 eddies detected in 2003–2007. EKE was weaker in the third period due to fewer observations. Southeastern (mooring D) EKE did not show apparent growth until the third period due to much stronger eddies detected. There were only 14 eddies in 2014–2018 and 24 eddies detected in 2008–2014. In short, there were either stronger eddies or more eddies after 2014 than before.

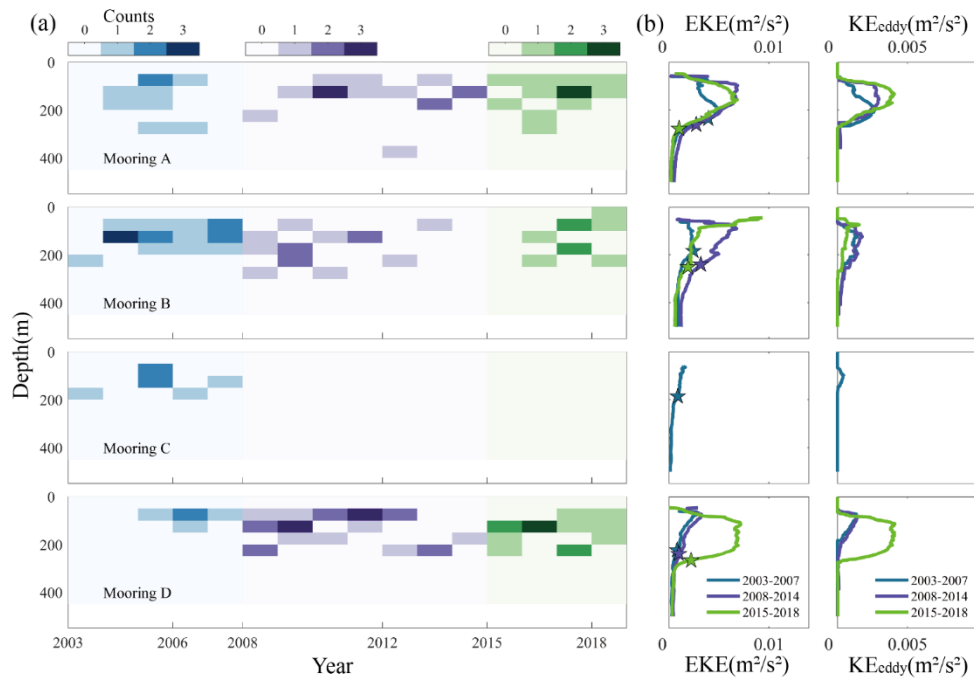
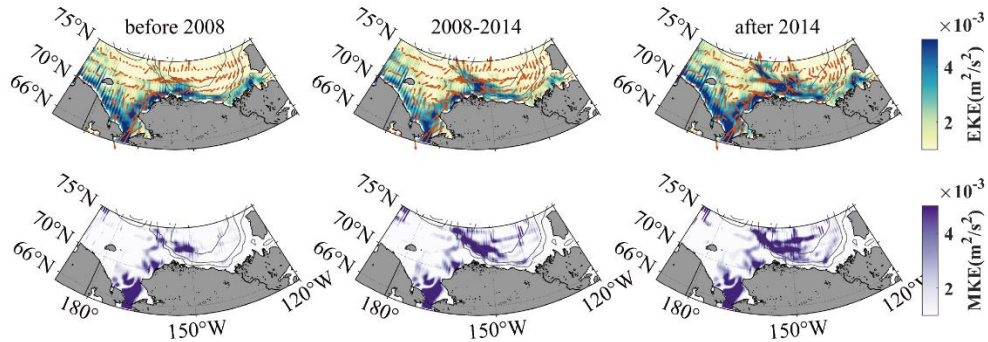


**Figure 6. (a) Hovmöller diagrams of depth against time showing annual eddy counts in the upper layer at moorings A–D. Blue, purple, and green shadings denote the spans of the three periods. (b) Interannual mean vertical profiles of eddy kinetic energy (EKE) and kinetic energy from eddies ( $KE_{\text{eddy}}$ ). Coloured stars indicate the depths of the halocline base in corresponding periods.**

## 325 4.2 Long-term EKE evolution from multiple datasets

The BG region, a focal area for mesoscale phenomena in previous studies (Armitage et al., 2020; Regan et al., 2020; Zhao and Timmermans, 2015; Zhao et al., 2016), mainly consists of a southern narrow continental shelf close to the Alaska coast and a sizable deep basin. The Chukchi–Beaufort slope is the major sector for eddy generation by baroclinic instability (Spall et al., 2008), with a surface front approximately along the 300 m isobath (Timmermans and Toole, 2023), and then eddies carrying Pacific water propagate to the central BG by the boundary current. Here, we focus on this area to investigate the interannual mean surface EKE patterns from a broad perspective by satellite-derived dynamic heights. As shown in Fig. 7, the high-value areas of EKE are mainly located along the continental slopes of the marginal CB especially the Alaska coast, mostly between the 1000 m and 3000 m isobaths. Indeed, energy is strongest at the southwestern shelf break of CB near the Barrow Cape, which can reach more than  $5 \times 10^{-3} \text{ m}^2/\text{s}^2$ , while it is even less than  $1 \times 10^{-3} \text{ m}^2/\text{s}^2$  in the interior basin. Notably, the horizontal pattern of EKE is not identical to that of mean kinetic energy (MKE) obtained by annual mean geostrophic current. Overall, the area with the highest EKE is closer to the inshore shelf seas than the area with the highest MKE. In every period, the EKE field along the southern continental slope was significantly enhanced compared with that in the previous period, and the strong EKE gradually developed from coasts to offshore regions and the central basin with time. For instance, from the interannual mean horizontal patterns, the region with the strongest EKE was mostly concentrated at the southern part of  $72^\circ\text{N}$  if we only noticed the section along the 1000 m isobath before 2007 (1993–2007) and it extended to approximately  $73^\circ\text{N}$  in the next period. Furthermore, the domain was even extended northwards up to  $74^\circ\text{N}$  lying at the Northwind Ridge delineated by a long, clear, and curved ribbon in the final period. We imply that eddy transportation contributes considerably to this development, which still needs additional evidence.

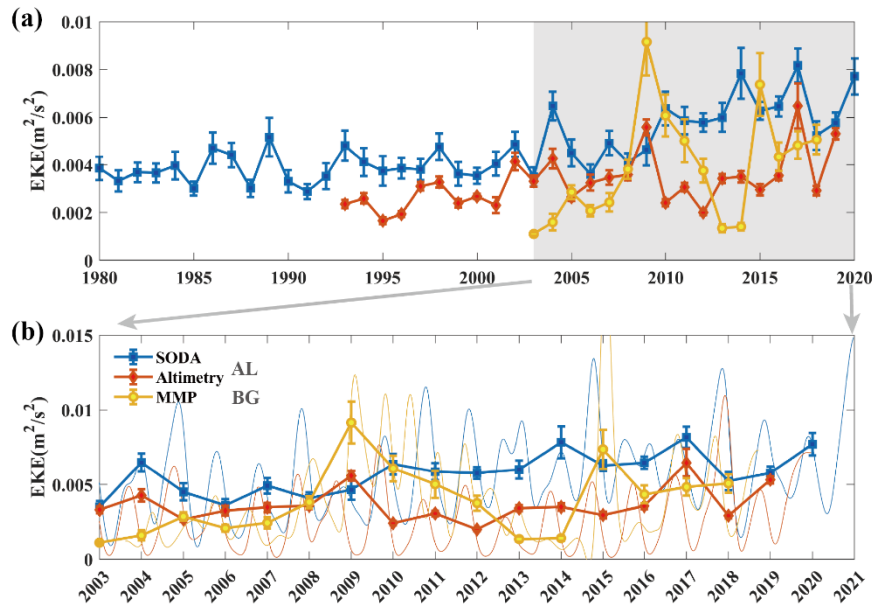


345 **Figure 7. Interannual mean maps of (upper panel) eddy kinetic energy (EKE) and (lower panel) mean kinetic energy (MKE) at the surface in 1993–2007 (before 2008), 2008–2014, and 2015–2019 (after 2014). Geostrophic current field is indicated by vectors.**

Currently, the seasonality of EKE in the Arctic is clear, generally stronger in summer or autumn and weaker in spring or winter (Wang et al., 2020; Manucharyan and Thompson, 2022), which is similar to other global regions (Rieck et al., 2015; Jia et al., 2011). Seasonal cycles of EKE in the central basin and basin boundary regions are both distinct (Fig. 8b). However, the

350 research on long-term EKE evolution is still limited. The Alaska coast and the Chukchi–Beaufort slope are the key areas of  
varying EKE (Fig. 7). In addition, we use finite datasets derived from SODA reanalysis, altimetry, and moored observations  
to explore the long-term variability in EKE between the central basin and continental slope. We select a western point of the  
Alaska coast called the AL region near the Barrow Cape (Fig. 1c) and the BG region represented by the positions of four  
355 et al., 2014). The variability of eddy counts in four moorings are also consistent with former research by ITP observations in  
four sectors of the CB (Zhao et al., 2016), so EKE above the halocline base for different moorings is vertically averaged with  
depth to comprehensively characterize the main features of eddy strength over the years between 2003 and 2018.

Based on the previous works, surface eddy activities are directly responding to the extra wind energy input (Armitage et al.,  
2020), while the subsurface EKE is related to from baroclinic instability and APE release (Manucharyan and Spall, 2016;  
360 Manucharyan et al., 2016). Eddy activities at the surface and subsurface are both linked with BG stabilisation, contributing to  
increased energy dissipation. Here the annual mean time series of surface EKE from SODA reanalysis (1980–2020) and  
altimetry (1993–2019) in the AL region and subsurface EKE from MMP (2003–2018) in the BG region are compared (Fig. 8).  
In the AL region, surface EKE was relatively weak before 2003, so we do not discuss it emphatically. EKE from altimetry has  
increased gradually since the 1990s and peaked in 2009, and then, it decreased in 2009–2010, resulting in relatively weak and  
365 stable EKE in 2010–2015. Although the EKE from reanalysis is the highest estimate among them, it has also increased since  
the 1990s and remained at a relatively stable level in 2010–2013. In the BG region, subsurface EKE began to increase rapidly  
since 2003 and peaked in 2009, and it indicated a decrease until 2014, which was slightly different from that in the AL region.  
When EKE was relatively strong after increasing, its cumulative effect was contributing to plateauing of halocline depth and  
weakening of halocline steepness associated with APE release. These characteristic shifts of eddy and oceanic stratification  
370 were both related to the varying physics of the gyre in the upper layer that indicated a strengthening during the years before  
2007 and a possible stabilisation since 2008 (Zhang et al., 2016). After experiencing a low ebb, especially from altimetry and  
MMP, since 2014/2015, EKE has presented some enhancements over time and remained at higher levels than in previous years  
before 2008 between the central BG and marginal AL regions.



375 **Figure 8. (a) Annual mean eddy kinetic energy (EKE) from MMP (2003–2018) averaged over 250 m in the BG region, altimetry (1993–2019), and SODA (1980–2020) at the surface in the AL region. Error bars represent 1/10 standard deviation in every year. (b) Annual mean EKE during 2003–2020 from partial results of (a). Thin lines are original time series smoothed by applying a 100-day low-pass filter.**

## 5 Eddy modulation in the asymmetrical halocline

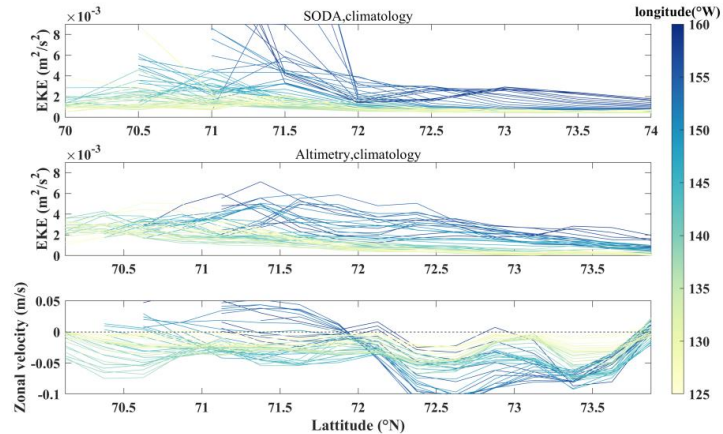
380 In the context of gyre variability and the most prominent sea ice losses in the BG region (Timmermans and Toole, 2023), extra wind energy input leads to more active eddies. Both surface and subsurface eddy activities are linked to gyre stability (Armitage et al., 2020; Manucharyan and Spall, 2016; Manucharyan et al., 2016). As discussed in sections 3 and 4, the halocline, as a measure of gyre stability, necessarily exhibits significant changes when eddy number and strength are enhanced under this background. In particular, the variability of the halocline in the BG region demonstrates an apparent reduction in meridional  
 385 asymmetry. How do eddies, as a key physical process, modulate the halocline in this phenomenon? In this section, we combine the variety of eddy number and strength analysed in section 4 with the varying asymmetry of the halocline to elucidate how eddy activities modulate in the halocline.

### 5.1 Relationship between geostrophic currents and EKE

The APE and geostrophic currents are both diagnostic variables of the halocline depth (Armitage et al., 2020). Eddies are  
 390 generated by dissipating APE, and they gradually weaken the slope of isopycnals as well as geostrophic currents. Furthermore, the seasonality of eddy and geostrophic current fields is similar in the Arctic surrounding seas (Armitage et al., 2017). EKE at the southwestern part of the basin with the confluence of reversed zonal geostrophic currents is the strongest (Fig. 9). The area with stronger (weaker) zonal currents is relatively weaker (stronger) EKE in the northern (southern) part of the Beaufort Sea



slope (BSS) region. Along the Alaska coast (south of 72°N), EKE is higher by approximately one order of magnitude than MKE, indicating EKE is dominant in this region, while in the offshore deep basin, MKE is one order of magnitude higher than EKE, which agrees with most areas in the Arctic Ocean (von Appen et al., 2022). After 2014, the domain with strong EKE has gradually departed from coasts (Fig. 7). Particularly, EKE has exceeded MKE near the central BG, representing the interior MKE was constrained.



400 **Figure 9. Climatology meridional eddy kinetic energy (EKE) from (upper panel) SODA reanalysis (1980–2020) and (middle panel) altimetry (1993–2019) in the Beaufort Sea slope (BSS) region. (lower panel) is the same as upper and middle panels but for climatology zonal geostrophic velocity.**

We compare the probability analysis results of EKE and geostrophic velocities averaged in the AL region based on the satellite altimetry in three periods (Fig. 10), which is estimated by the statistical frequency of the area mean time series in every period. 405 The annual mean EKE was significantly intensified by 17% (26%) from period 1 to period 2 (from period 2 to period 3). Furthermore, its main values within the extent with a probability of 68.4% were also enhanced. Although the velocities were both increased in the last two periods, the magnitudes of their increases were only 15% and 7%, which are much smaller than that of EKE. When the EKE in this region continued to sharply increase in the past, the velocity field increased more slowly. The rate of velocity change began to decrease, while EKE was still increasing rapidly, representing that the difference between 410 them has been magnified in recent years. For further clarification, we explore the relationship between these two variables. In addition, we find that these variabilities show a strong correlation over the area of interest (Fig. 10g). The correlation coefficients between EKE and local geostrophic velocities are mainly negative near the Alaska coast and partial central basin, which is verified by their variation in the AL region. However, the major correlation coefficients passing the significance test level of 95% remain highly positive between the 1000 m and 3000 m isobaths along the southwestern margins of the basin, 415 which is likely caused by the continuously enhanced EKE offshore even emerging in the deep basin.

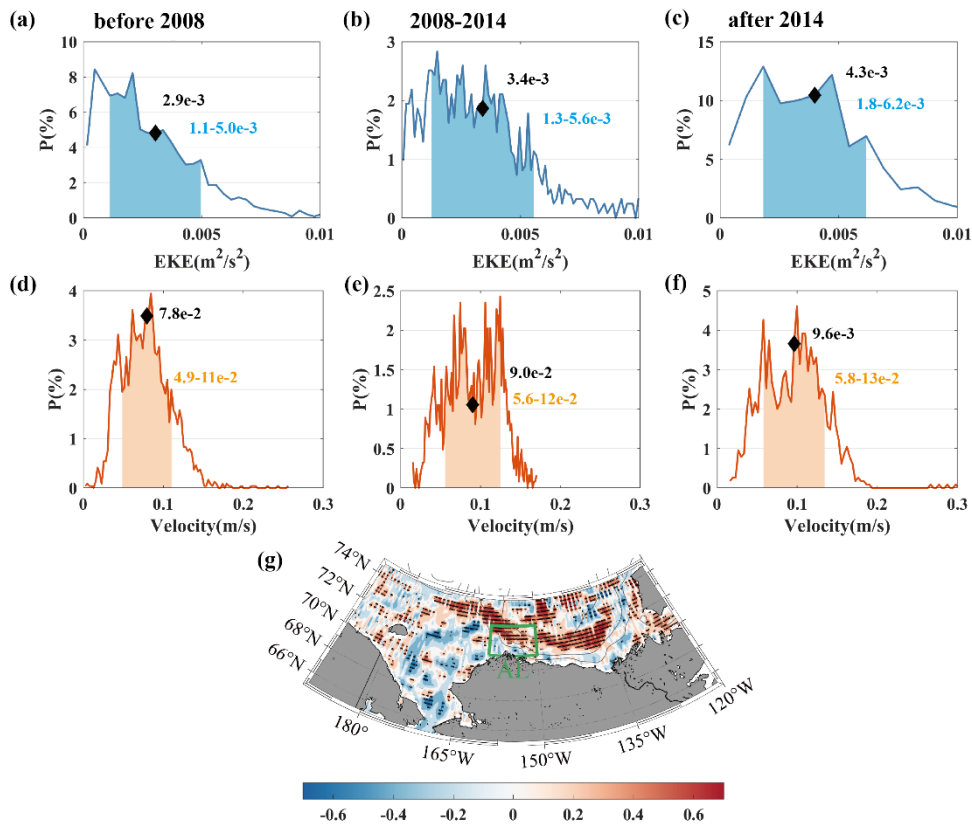
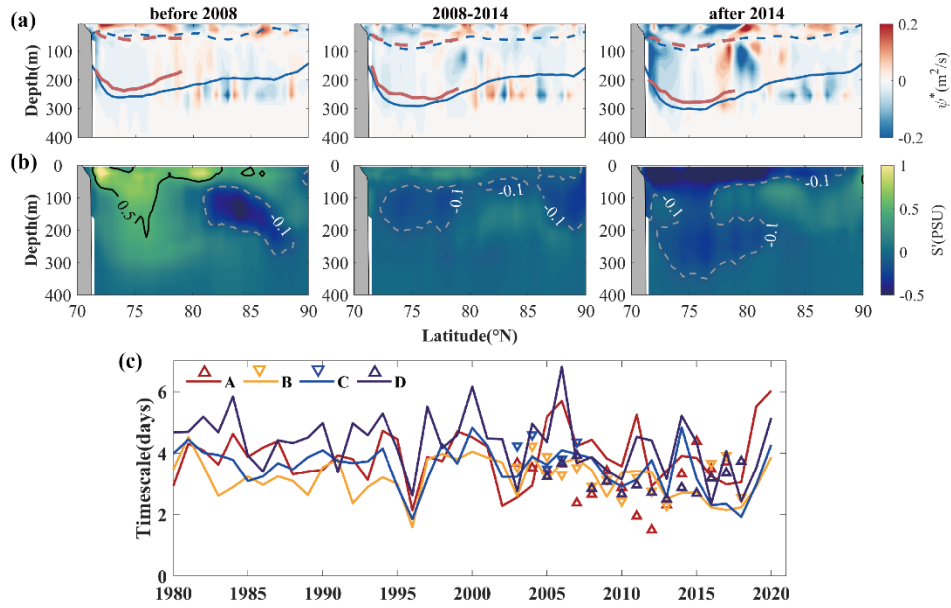


**Figure 10. Probability of (a–c) eddy kinetic energy (EKE) and (d–e) geostrophic velocity in the Alaskan coast (AL) region during (a, d) 1993–2007, (b, e) 2008–2014, and (c, f) 2015–2019. Black diamonds represent mean values in three periods. The range of shading indicates the extent with a probability of 68.4%. (g) A map of the correlation coefficients between the annual mean eddy kinetic energy (EKE) and local geostrophic velocities in 1993–2019. Black dots indicate all positions that passed a significance test (confidence level 95%).**

## 5.2 Eddy lateral flux: a critical role in modulating the halocline

In recent years, after APE continuously decreased during 2010–2014, EKE has remained at a relatively strong level compared with the mean value over the whole period. In the meantime, the meridional asymmetry of the halocline geometry reduced, and the increasing rate of geostrophic currents slowed down. It is currently known that eddies can not only dissipate APE but also hinder freshwater accumulation. The halocline vertical structure has tended to be meridionally symmetrical in the BG region in recent years, which was proven by observations and SODA reanalysis. The varying structure can be well replicated through SODA reanalysis schematically (Fig. 11a), although the results from SODA overestimate the depth of the halocline to a certain extent with an error of 30–40 m near the central basin. The changes in the halocline structure at each side in the three periods obtained from SODA showed a strong consistency with the results from the CTD, which verified that the northern halocline of central gyre was shallower and flatter than the southern part before 2008 and the halocline at each side along the meridional transect remained at a similar level after 2014.



435 **Figure 11. Transects of (a) eddy stream function and (b) salinity anomaly relative to the whole term averaged in 2004–2007 (before 2008), 2008–2014 and 2015–2020/2021 (after 2014), calculated from SODA simulated now until 2020 and CTD observed until 2021. The dashed (solid) lines indicate the processed annual mean depth of isopycnal surface  $\sigma = 25$  (27.4)  $\text{kg} \cdot \text{m}^{-3}$  representing the halocline top (base) from SODA (blue lines, selected data are from September to October, which is mostly consistent with the observed data for CTD deployment) and CTD (red lines) during three periods. (c) Annual mean time series of the Eady timescale calculated from SODA (solid line) and MMP (triangle) at four moorings.**

440 Aiming to explore the critical role that eddies play in the halocline, we analyse the eddy stream function evaluated by Eq. (5) over a long-term scale based on SODA. In the first period, when the Eady timescale was relatively larger over the long term (Fig. 11c), meaning stronger stability, the salinity anomalies in the mixed layer and the halocline layer were both positive, more than 0.5 (Fig. 11b). Combined with the distribution pattern of the eddy stream function, the eddy thickness fluxes were generally positive at the surface, about  $0.1 \text{ m}^2/\text{s}^2$ , and represented the southwards (northwards) propagation of low-salinity (high-salinity) water. However, in the halocline layer, stronger eddy fluxes were mainly distributed at the southern and northern edges of the gyre, finally resulting in a northern high-salinity anomaly and southern halocline much deeper than the north at the same time. In the second period, when a transformation took place in the upper layer, the Eady timescale decreased, indicating enhanced baroclinic instability in the BG. There were low-salinity anomalies of about  $-0.2$  in the halocline layer, and eddy thickness fluxes of less than  $-0.1 \text{ m}^2/\text{s}^2$  indicated a northwards propagation of low-salinity water. In the meantime, there was an overall deepening of the halocline depth. In the third period, significantly low-salinity anomalies in the halocline were in the upper layer of BG region. In addition, the main spatial pattern of eddy flux in this period was extremely similar to that in the former period but with obvious strengthening. In the mixed layer, the eddy thickness fluxes were less than  $-0.2 \text{ m}^2/\text{s}^2$ . The eddy-induced low-salinity water transportations replenished the freshwater in the north. In the halocline layer, among  $71$ – $79^\circ\text{N}$  surrounding the gyre center, the convergence of eddy lateral fluxes was extremely strong. Eddy fluxes were less than  $-0.1 \text{ m}^2/\text{s}^2$  on the southern edge and more than  $0.1 \text{ m}^2/\text{s}^2$  on the northern edge, meaning that low-salinity water at the subsurface

445

in the south near the continental slope spread northwards, but in the north it spread southwards, which formed a central-converging pattern. The freshwater redistribution induced by eddy lateral flux, with the location of central gyre far from south, contributed to the significantly flatter and inflated halocline surrounding gyre center, which led to reduced asymmetry. Some of the low-salinity water continued to spread northwards, which coincided with the northward expansion and release of the  
460 freshwater from gyre mentioned in a recent study (Bertosio et al., 2022).

## 6 Summary and discussion

Our main objective is to explore how long-term variations in eddy activity influence the spatiotemporal variability in the halocline under the BG system. In this study, our analyses of the halocline based on in situ hydrologic data including MMP from moored observations and CTD from BGEP, both showed that the northern and southern depths of isopycnals around  
465 central gyre have deepened to different degrees in nearly the last two decades. The halocline depth significantly increased in the deep basin and continental slopes (Kenigson et al., 2021; Zhong et al., 2019). The halocline in the south deepened by ~40 m, while that in the north deepened by ~70 m over the years 2003–2018. After 2014, when gyre center removed to far from southern edge, the difference in halocline depth and thickness at either side of the central gyre was smaller than before. The meridional asymmetry of the halocline with halocline depth lifting to the north that induced a thinner halocline thickness in  
470 the north was initially shifted to a final nearly symmetrical structure surrounding central gyre.

Furthermore, we investigated the spatiotemporal variability of eddies and EKE between the central gyre and continental slope to try to clarify why the halocline changed asymmetrically. There were 37, 40, 7, and 43 eddies detected in the upper layer at moorings A–D, 98% of which were anticyclones. The EKE at the southwestern corner was much stronger after 2008 than in the previous period, but it remained relatively stable later, which was consistent with the declined Eady timescale. With  
475 halocline depth varying, the number and strength of eddies at different sites as well as EKE at key regions exhibit considerable interannual fluctuations. There are more active and stronger eddies in the final period than before. The difference in eddy activity at each site is affected by spatial inhomogeneity of eddy distribution or eddy transportation from the southern BG region where they are generated. The highest EKE region is close to the reversal currents with relatively weaker mean flows there. When EKE is enhanced along the Chukchi/Beaufort continental slope, it gradually develops towards the abyssal plain,  
480 which agrees with its intensification in the interior gyre in the final period from observations because of APE release. Surface and subsurface eddy activities jointly influenced oceanic stratification by inhibiting surface mean flows and promoting APE release above the halocline layer related to BG stabilisation. Under increased eddy modulation provided by multiple datasets in the BG region, the halocline depth experienced a deepening and then a shallowing or stagnate phase in the BG region, and the increase in geostrophic flows also slowed down. Notably, the high EKE region was close to the reversal currents with  
485 relatively weak flows there.

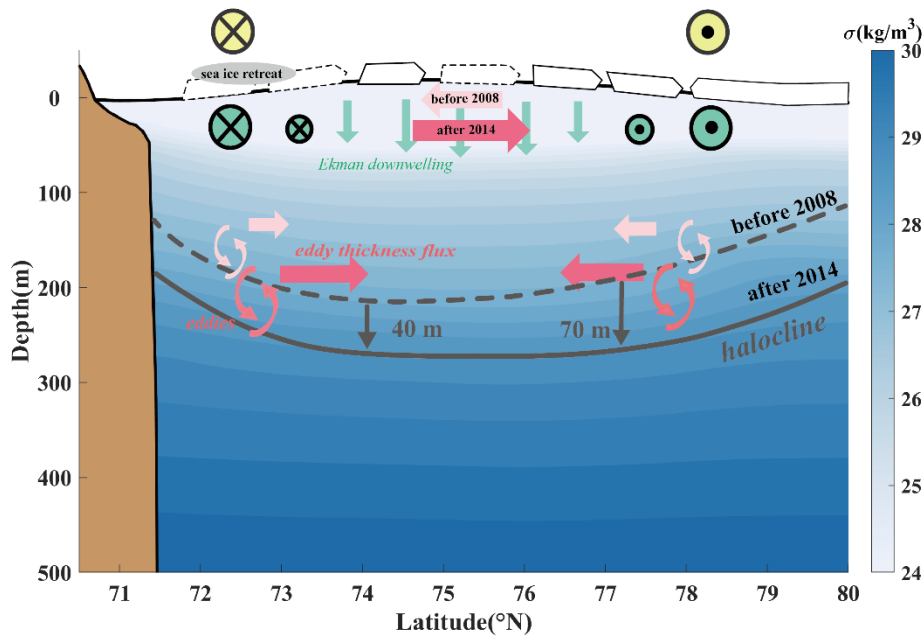


**Figure 12.** The schematic diagram under the BG system referred to the transect of  $150^{\circ}\text{W}$ , indicating the recent eddy modulation in the halocline. Shading is the climatology potential density from 1990–2020 WOA climatology. Light (Dark) green arrows represent the eddy thickness momentum before 2008 (after 2014).

490 Many studies support that BG system is strongly affected by atmospheric dynamics that contribute to deeper halocline in the interior gyre. The center of the surface sea level dome and wind-forced Ekman pumping area are also highly sensitive to wind patterns (Manucharyan and Spall, 2016; Regan et al., 2019; Timmermans and Toole, 2023). In this study, the deformation in the main features of halocline around central gyre are investigated. Overall, the credible results revealed that the eddy fluxes, playing a critical role in modulating the halocline, have adjusted the vertical structure of the halocline by affecting the

495 freshwater redistribution in the past years comparing the initial period with the final period (Fig. 12). Currently, meridional asymmetry of the BG halocline is distinctly diminished due to strengthened modulation of the eddy lateral flux. For the first period, the eddy fluxes were mostly positive in the surface mixed layer, indicating the southwards propagation of freshwater, which explained the tilted structure of the halocline with the largest steepness in the southern edge. In the final period, the eddy fluxes above the mixed layer were remarkably negative, indicating the northwards transportations of freshwater, and an

500 extremely strong convergent center was formed in the halocline layer. A series of processes promoted the surface low-salinity water transportations to the north and it can be beneficial for freshwater confluence in the halocline at depth from two sides, which adjusted the deformation of the halocline structure.

To date, previous studies hypothesised that the accumulation of freshwater driven by Ekman pumping is balanced by the effect of mesoscale eddies for stabilising the circulation (e.g., Davis et al., 2014; Manucharyan and Spall, 2016), not yet probing too

505 much of the spatial difference in the halocline structure. This paper provides a possible perspective for understanding the long-term changes in the stratification structure and eddy field in the BG and the relationship between them. We expect it to further

the knowledge of large-scale circulation and mesoscale processes under the background of rapid changes in the Arctic. It is still necessary to use high-resolution simulations combined with observations across the gyre to obtain a comprehensive understanding of interior variations between different physical processes, for promoting scientific development in BG dynamics.

### **Data availability**

The gridded satellite altimeter data (product identifier: SEALEVEL\_GLO\_PHY\_L4\_REP\_OBSERVATIONS\_088\_047) is freely made available by the Copernicus Marine Environmental Monitoring Service (<https://data.marine.copernicus.eu/products>). Observations including CTD and MMP profiles are collected and made available by the Beaufort Gyre Exploration Project based at the Woods Hole Oceanographic Institution (<https://www2.whoi.edu/site/beaufortgyre>) in collaboration with researchers from Fisheries and Oceans Canada at the Institute of Ocean Sciences. SODA is from the Ocean Climate Lab at the University of Maryland (<https://www2.atmos.umd.edu/~ocean/index.htm>).

### **Author contribution**

LD provided the initial scientific idea and financial supports. LD and JL together conceived the idea for the present study. JL and ST collected all available datasets. JL processed the data, plotted the results, and wrote the first version of the manuscript. All authors reviewed and edited the manuscript to its final version.

### **Competing interests**

The authors declare that they have no conflicts of interest.

### **Acknowledgements**

Thank you to the two anonymous reviewers for their helpful comments and valuable suggestions, which greatly improved this manuscript. The authors acknowledge Service Woods Hole Oceanographic Institution for making mooring data and in situ observations available. We thank the Copernicus Marine Environmental Monitoring for providing altimetry data. We appreciate the Ocean Climate Lab at the University of Maryland for providing data assimilation.

## 530 **Financial support**

This study is supported by the National Natural Science Foundation of China (NSFC, grant no. 41576020, 42076228, and 42230405).

## **References**

- Aagaard, K., Coachman, L. K., and Carmack, E.: On the halocline of the Arctic Ocean. *Deep-sea Res.*, 28, 529-545. [https://doi.org/10.1016/0198-0149\(81\)90115-1](https://doi.org/10.1016/0198-0149(81)90115-1), 1981.
- 535 Armitage, T. W. K., Bacon, S., Ridout, A. L., Petty, A. A., Wolbach, S., and Tsamados, M.: Arctic Ocean surface geostrophic circulation 2003-2014, *Cryosphere*, 11, 1767-1780. <https://doi.org/10.5194/tc-11-1767-2017>, 2017.
- Armitage, T., Manucharyan, G. E., Petty, A. A., Kwok, R., and Thompson, A. F.: Enhanced eddy activity in the Beaufort Gyre in response to sea ice loss. *Nat. Commun.*, 11, 1-8. <https://doi.org/10.1038/s41467-020-14449-z>, 2020.
- 540 Bertosio, C., Provost, C., Athanase, M., Sennéchaël, N., Garric, G., Lellouche, J. M., Bricaud, C., Kim, J. H., Cho, K. H., and Park, T.: Changes in freshwater distribution and pathways in the Arctic Ocean since 2007 in the mercator ocean global operational system. *J. Geophys. Res. Oceans*, 127, e2021JC017701. <https://doi.org/10.1029/2021JC017701>, 2022.
- Bourgain, P., and Gascard, J. C.: The Arctic Ocean halocline and its interannual variability from 1997 to 2008. *Deep-sea Res.*, 58, 745-756. <https://doi.org/10.1016/j.dsr.2011.05.001>, 2011.
- 545 Chelton, D. B., Schlax, M. G., Samelson, R. M., and de Szoeke, R. A.: Global observations of large oceanic eddies. *Geophys. Res. Lett.*, 34, L15606. <https://doi.org/10.1029/2007GL030812>, 2007.
- Davis, P. E. D., Lique, C., and Johnson, H. L.: On the link between arctic sea ice decline and the freshwater content of the Beaufort Gyre: Insights from a simple process model. *J. Clim.*, 27, 8170-8184. <https://doi.org/10.1175/JCLI-D-14-00090.1>, 2014.
- 550 Doddridge, E. W., Meneghello, G., Marshall, J., Scott, J., and Lique, C.: A Three-way balance in the Beaufort Gyre: The Ice-Ocean Governor, wind stress, and eddy diffusivity. *J. Geophys. Res. Oceans*, 124, 3107-3124. <https://doi.org/10.1029/2018JC014897>, 2019.
- Fer, I., Bosse, A., Ferron, B., and Bouruet-Aubertot, P.: The dissipation of kinetic energy in the Lofoten Basin eddy. *J. Phys. Oceanogr.*, 48, 1299-1316. <https://doi.org/10.1175/JPO-D-17-0244.1>, 2018.
- 555 Giles, K. A., Laxon, S. W., Ridout, A. L., Wingham, D. J., and Bacon, S.: Western Arctic Ocean freshwater storage increased by wind-driven spin-up of the Beaufort Gyre. *Nat. Geosci.*, 5, 194-197. <https://doi.org/10.1038/ngeo1379>, 2012.
- Huang, R. X.: Mixing and available potential energy in a Boussinesq ocean. *J. Phys. Oceanogr.*, 28, 669-678. [https://doi.org/10.1175/1520-0485\(1998\)028<0669:MAAPEI>2.0.CO;2](https://doi.org/10.1175/1520-0485(1998)028<0669:MAAPEI>2.0.CO;2), 1998.
- Huang, J., Zhang, X., Zhang, Q., Lin, Y., Hao, M., Luo, Y., Zhao, Z., Yao, Y., Chen, X., Wang, L., Nie, S., Yin, Y., Xu, Y., and Zhang, J.: Recently amplified arctic warming has contributed to a continual global warming trend. *Nat. Clim. Change.*, 7, 875-879. <https://doi.org/10.1038/s41558-017-0056-y>, 2018.
- 560

- Jia, F., Wu, L., and Qiu, B.: Seasonal modulation of eddy kinetic energy and its formation mechanism in the southeast Indian Ocean. *J. Geophys. Res. Oceans*, 41, 657-665. <https://doi.org/10.1175/2010JPO4436.1>, 2011.
- 565 Karcher, M., Kauker, F., Gerdes, R., Hunke, E. and Zhang, J: On the dynamics of Atlantic Water circulation in the Arctic Ocean. *Journal of Geophysical Research*, 112, C04S02, <https://doi.org/10.1029/2006JC003630> , 2007
- Kenigson, J. S., Gelderloos, R., and Manucharyan, G. E.: Vertical structure of the Beaufort Gyre halocline and the crucial role of the depth-dependent eddy diffusivity. *J. Phys. Oceanogr.*, 51, 845-860. <https://doi.org/10.1175/JPO-D-20-0077.1>, 2021.
- Kozlov, I. E., Artamonova, A. V., Manucharyan, G. E., and Kubryakov, A. A.: Eddies in the western Arctic Ocean from spaceborne SAR observations over open ocean and marginal ice zones. *J. Geophys. Res. Oceans*, 124, 6601-6616. 570 <https://doi.org/10.1029/2019JC015113>, 2019.
- Krishfield, R. A., Proshutinsky, A., Tateyama, K., Williams, W. J., Carmack, E. C., McLaughlin, F. A., and Timmermans, M. L.: Deterioration of perennial sea ice in the Beaufort Gyre from 2003 to 2012 and its impact on the oceanic freshwater cycle. *J. Geophys. Res. Oceans*, 119, 1271-1305. <https://doi.org/10.1002/2013JC008999>, 2014.
- Kubryakov, A. A., Kozlov, I. E., and Manucharyan, G. E.: Large mesoscale eddies in the western Arctic Ocean from Satellite 575 altimetry measurements. *J. Geophys. Res. Oceans*, 126, e2020JC016670. <https://doi.org/10.1029/2020JC016670>, 2021.
- Luecke, C. A., Arbic, B. K., Bassette, S. L., Richman, J. G., Shriver, J. F., Alford, M. H., Smedstad, O. M., Timko, P. G., Trossman, D. S., and Wallcraft, A. J.: The global mesoscale eddy available potential energy field in models and observations. *J. Geophys. Res. Oceans*, 122, 9126-9143. <https://doi.org/10.1002/2017JC013136>, 2017.
- Manley, T. O., and Hunkins, K.: Mesoscale eddies of the Arctic Ocean. *J. Geophys. Res. Oceans*, 90, 4911- 580 4930. <https://doi.org/10.1029/JC090iC03p04911>, 1985.
- Manucharyan, G. E., and Timmermans, M.: Generation and separation of mesoscale eddies from surface ocean fronts. *J. Phys. Oceanogr.*, 43, 2545-2562. <https://doi.org/10.1175/JPO-D-13-094.1>, 1985, 2013.
- Manucharyan, G. E., and Spall, M. A.: Wind-driven freshwater buildup and release in the Beaufort Gyre constrained by mesoscale eddies. *Geophys. Res. Lett.*, 43, 273-282. <https://doi.org/10.1002/2015GL065957>, 2016.
- 585 Manucharyan, G. E., Spall, M. A., and Thompson, A. F.: A theory of the wind-driven Beaufort Gyre variability. *J. Phys. Oceanogr.*, 46, 3263-3278. <https://doi.org/10.1175/JPO-D-16-0091.1>, 2016.
- Manucharyan, G. E., Thompson, A. F., and Spall, M. A.: Eddy memory mode of multidecadal variability in residual-mean ocean circulations with application to the Beaufort Gyre. *J. Phys. Oceanogr.*, 47, 855-866. <https://doi.org/10.1175/JPO-D-16-0194.1>, 2017.
- 590 Manucharyan, G. E., and Isachsen, P. E.: Critical role of continental slopes in halocline and eddy dynamics of the Ekman-driven Beaufort Gyre. *J. Geophys. Res. Oceans*, 124, 2679-2696. <https://doi.org/10.1029/2018JC014624>, 2019.
- Manucharyan, G. E. and Stewart, A. L.: Stirring of interior potential vorticity gradients as a formation mechanism for large subsurface-intensified eddies in the Beaufort Gyre. *J. Phys. Oceanogr.*, 52, 3349-3370, <https://doi.org/10.1175/JPO-D-21-0040.1>, 2022.



- 595 Manucharyan, G. E., and Thompson, A. F.: Heavy footprints of upper-ocean eddies on weakened Arctic sea ice in marginal ice zones. *Nat. Commun.*, 13, 1-10. <https://doi.org/10.1038/s41467-022-29663-0>, 2022.
- Marshall, J., and Radko, T.: Residual-mean solutions for the Antarctic Circumpolar Current and its associated overturning circulation. *J. Phys. Oceanogr.*, 33, 2341-2354. [https://doi.org/10.1175/1520-0485\(2003\)033<2341:RSFTAC>2.0.CO;2](https://doi.org/10.1175/1520-0485(2003)033<2341:RSFTAC>2.0.CO;2), 2003.
- 600 McLaughlin, F. A., Carmack, E. C., Macdonald, R. W., Melling, H., Swift, J. H., Wheeler, P. A., Sherr, B. F. and Sherr, E. B.: The joint roles of Pacific and Atlantic-origin waters in the Canada Basin, 1997–1998. *Deep-sea Res.*, 51, 107-128. <https://doi.org/10.1016/j.dsr.2003.09.010>, 2004.
- Meneghello, G., Marshall, J., Lique, C., Isachsen, P. E., Doddridge, E., Campin, J., Regan, H., and Talandier, C.: Genesis and decay of mesoscale baroclinic eddies in the seasonally ice-covered interior Arctic Ocean. *J. Phys. Oceanogr.*, 51, 115-605 129. <https://doi.org/10.1175/JPO-D-20-0054.1>, 2021.
- Moore, G. W. K., Schweiger, A., Zhang, J., and Steele, M.: Collapse of the 2017 winter Beaufort High: a response to thinning sea ice? *Geophys. Res. Lett.*, 45, 2860-2869. <https://doi.org/10.1002/2017GL076446>, 2018.
- Munk, W., and Wunsch, C.: Abyssal recipes II: Energetics of tidal and wind mixing. *Deep-sea. Res.*, 45, 1977-2010. [https://doi.org/10.1016/S0967-0637\(98\)00070-3](https://doi.org/10.1016/S0967-0637(98)00070-3), 1998.
- 610 Niederrenk, A. L., and Notz, D.: Arctic sea ice in a 1.5°C warmer world. *Geophys. Res. Lett.*, 45, 1963-1971. <https://doi.org/10.1002/2017GL076159>, 2018.
- Penduff, T., Barnier, B., Dewar, W. K., and O'Brien, J. J.: Dynamical response of the oceanic eddy field to the North Atlantic Oscillation: a model-data comparison. *J. Phys. Oceanogr.*, 34, 2615-2629. <https://doi.org/10.1175/JPO2618.1>, 2004.
- Polyakov, I. V., Pnyushkov, A. V., and Carmack, E. C.: Stability of the Arctic halocline: a new indicator of Arctic climate 615 change. *Environ. Res. Lett.*, 13, 125008. <https://doi.org/10.1088/1748-9326/aaec1e>, 2018.
- Proshutinsky, A., Krishfield, R., Timmermans, M., Toole, J., Carmack, E., McLaughlin, F., Williams, W. J., Zimmermann, S., Itoh, M., and Shimada, K.: Beaufort Gyre freshwater reservoir: State and variability from observations, *J. Geophys. Res. Oceans*, 114, C00A10, <https://doi.org/10.1029/2008JC005104>, 2009.
- Proshutinsky, A., Krishfield, R., Toole, J. M., Timmermans, M. L., Williams, W., Zimmermann, S., Yamamoto Kawai, M., 620 Armitage, T. W. K., Dukhovskoy, D., Golubeva, E., Manucharyan, G. E., Platov, G., Watanabe, E., Kikuchi, T., Nishino, S., Itoh, M., Kang, S. H., Cho, K. H., Tateyama, K., and Zhao, J.: Analysis of the Beaufort Gyre freshwater content in 2003-2018. *J. Geophys. Res. Oceans*, 124, 9658-9689. <https://doi.org/10.1029/2019JC015281>, 2019.
- Raj, R. P., Johannessen, J. A., Eldevik, T., Nilsen, J. E. O., and Halo, I.: Quantifying mesoscale eddies in the Lofoten Basin. *J. Geophys. Res. Oceans*, 121, 4503-4521. <https://doi.org/10.1002/2016JC011637>, 2016.
- 625 Regan, H. C., Lique, C., and Armitage, T. W. K. : The Beaufort Gyre extent, shape, and location between 2003 and 2014 from Satellite observations. *J. Geophys. Res. Oceans*, 124, 844-862. <https://doi.org/10.1029/2018JC014379>, 2019.
- Regan, H., Lique, C., Talandier, C., and Meneghello, G.: Response of total and eddy kinetic energy to the recent spin-up of the Beaufort Gyre. *J. Phys. Oceanogr.*, 50, 575-594. <https://doi.org/10.1175/JPO-D-19-0234.1>, 2020.

- Rieck, J. K., Böning, C. W., Greatbatch, R. J., and Scheinert, M.: Seasonal variability of eddy kinetic energy in a global high-resolution ocean model. *Geophys. Res. Lett.*, 42, 9379-9386. <https://doi.org/10.1002/2015GL066152>, 2015.
- Rieck, J. K., Böning, C. W., and Greatbatch, R. J.: Decadal variability of eddy kinetic energy in the South Pacific Subtropical Countercurrent in an ocean general circulation model. *J. Phys. Oceanogr.*, 48, 757-771. <https://doi.org/10.1175/JPO-D-17-0173.1>, 2018.
- Serreze, M. C., and Barry, R. G.: Processes and impacts of Arctic amplification: A research synthesis. *Global Planet. Change.*, 77, 85-96. <https://doi.org/10.1016/j.gloplacha.2011.03.004>, 2011.
- Shimada, K., Itoh, M., Nishino, S., McLaughlin, F., Carmack, E., and Proshutinsky, A.: Halocline structure in the Canada Basin of the Arctic Ocean. *Geophys. Res. Lett.*, 32, L03605. <https://doi.org/10.1029/2004GL021358>, 2005.
- Smith, K. S.: The geography of linear baroclinic instability in Earth's oceans. *J. Mar. Res.*, 65, 655-683. <https://doi.org/10.1357/002224007783649484>, 2007.
- Spall, M. A., Pickart, R. S., Fratantoni, P. S., and Plueddemann, A. J.: Western Arctic Shelfbreak eddies: Formation and Transport. *J. Phys. Oceanogr.*, 38, 1644-1668. <https://doi.org/10.1175/2007JPO3829.1>, 2008.
- Stroeve, J., Holland, M. M., Meier, W., Scambos, T., and Serreze, M.: Arctic sea ice decline: Faster than forecast. *Geophys. Res. Lett.*, 34, L9501. <https://doi.org/10.1029/2007GL029703>, 2007.
- Stroeve, J. C., Markus, T., Boisvert, L., Miller, J., and Barrett, A.: Changes in Arctic melt season and implications for sea ice loss. *Geophys. Res. Lett.*, 41, 1216-1225., 2014.
- Timmermans, M. L., Toole, J., Proshutinsky, A., Krishfield, R., and Plueddemann, A.: Eddies in the Canada Basin, Arctic Ocean, observed from Ice-Tethered Profilers. *J. Phys. Oceanogr.*, 38, 133-145. <https://doi.org/10.1175/2007JPO3782.1>, 2008.
- Timmermans, M. L., and Marshall, J.: Understanding Arctic Ocean circulation: a review of ocean dynamics in a changing climate. *J. Geophys. Res. Oceans*, 125, e2018JC014378. <https://doi.org/10.1002/2013GL058951>, 2020.
- Timmermans, M., and Toole, J. M.: The Arctic Ocean's Beaufort Gyre. *Annu. Rev. Mar. Sci.*, 15, 223-248. <https://doi.org/10.1146/annurev-marine-032122-012034>, 2023.
- von Storch, J. S., Eden, C., Fast, I., Haak, H., Hernández-Deckers, D., Maier-Reimer, E., Marotzke, J., and Stammer, D.: Eddies and the distribution of eddy kinetic energy in the Arctic Ocean. *Oceanogr.* <https://doi.org/10.5670/oceanog.2022.122>, 2022.
- Wang, Q., Koldunov, N. V., Danilov, S., Sidorenko, D., Wekerle, C., Scholz, P., Bashmachnikov, I. L., and Jung, T.: Eddy kinetic energy in the Arctic Ocean from a global simulation with a 1-km Arctic. *Geophys. Res. Lett.*, 47, e2020GL088550. <https://doi.org/10.1029/2020GL088550>, 2020.
- Zhang, J., Steele, M., Runciman, K., Dewey, S., Morison, J., Lee, C., Rainville, L., Cole, S., Krishfield, R., Timmermans, M., and Toole, J.: The Beaufort Gyre intensification and stabilization: A model-observation synthesis, *J. Geophys. Res. Oceans*, 121, 7933-7952. <https://doi.org/10.1002/2016JC012196>, 2016.

- Zhang, J., Cheng, W., Steele, M., and Weijer, W.: Asymmetrically stratified Beaufort Gyre: mean state and response to decadal forcing. *Geophys. Res. Lett.*, 50. e2022GL100457. <https://doi.org/10.1029/2022GL100457>, 2023.
- 665 Zhao, M., Timmermans, M., Cole, S., Krishfield, R., Proshutinsky, A., and Toole, J.: Characterizing the eddy field in the Arctic Ocean halocline. *J. Geophys. Res. Oceans*, 119, 8800-8817. <https://doi.org/10.1002/2014JC010488>, 2014.
- Zhao, M., and Timmermans, M. L.: Vertical scales and dynamics of eddies in the Arctic Ocean's Canada Basin. *J. Geophys. Res. Oceans*, 120, 8195-8209. <https://doi.org/10.1002/2015JC011251>, 2015.
- Zhao, M., Timmermans, M., Cole, S., Krishfield, R., and Toole, J.: Evolution of the eddy field in the Arctic Ocean's Canada Basin, 2005-2015. *Geophys. Res. Lett.*, 43, 8106-8114. <https://doi.org/10.1002/2016GL069671>, 2016.
- 670 Zhao, M., Timmermans, M. L., Krishfield, R., and Manucharyan, G.: Partitioning of kinetic energy in the Arctic Ocean's Beaufort Gyre. *J. Geophys. Res. Oceans*, 123, 4806-4819. <https://doi.org/10.1029/2018JC014037>, 2018.
- Zhong, W., Steele, M., Zhang, J., and Cole, S. T.: Circulation of Pacific Winter Water in the western Arctic Ocean. *J. Geophys. Res. Oceans*, 124, 863-881. <https://doi.org/10.1029/2018JC014604>, 2019.